Physica Medica 60 (2019) 156–161

Contents lists available at ScienceDirect

Physica Medica

journal homepage: www.elsevier.com/locate/ejmp

Original paper

Dwell time verification in brachytherapy based on time resolved *in vivo* dosimetry

J.G. Johansen[a,*], G. Kertzscher[a], E.B. Jørgensen[a], S. Rylander[a], L. Bentzen[a], S.B. Hokland[a], C.S. Søndergaard[a], A.K.M. With[b], S. Buus[a], K. Tanderup[a]

[a] Department of Oncology, Aarhus University Hospital, DK-8000 Aarhus C, Denmark
[b] Örebro University Hospital, Örebro, Sweden

ARTICLE INFO

Keywords:
In vivo dosimetry
HDR brachytherapy
Prostate cancer
Treatment verification
Dwell times

ABSTRACT

Purpose: This paper presents a method to verify dwell times during High Dose Rate (HDR) Brachytherapy (BT) by means of *in vivo* dosimetry (IVD), and reports on an afterloader's stability in dwell time control.
Methods: *In vivo* dosimetry was performed during 20 HDR prostate cancer treatments using a point detector based on a radio-luminescence crystal (Al_2O_3:C) coupled to a fiber-optic cable. The dose rate was recorded at either 10 Hz or 20 Hz during the treatments. The "time of transit" when the source moved between two dwell positions was identified using the difference in count rate between two measurements. The dwell times were then determined by subtracting two adjacent times of transit. The measured dwell times were matched with the planned dwell times and categorised into two groups: Dwell times matching a single dwell position (identified) and dwell times matching the sum of multiple dwell positions (unidentified). Deviations between measured and planned dwell times were calculated for the identified dwell positions.
Results: A total of 3518 dwell positions were analysed. The amount of identified dwell positions were 82%, which increased to 89% if the short dwell times (< 1 s) were omitted in the analysis. The largest deviation was −0.4 s seen for a single dwell position, and in 97.1% of the cases, the deviations were < 0.15 s.
Conclusion: The dwell times in BT are well controlled by the afterloader. It is shown that IVD facilitates the detection of dwell time offsets that could have a clinical impact.

1. Introduction

In brachytherapy (BT), *in vivo* dosimetry (IVD) has traditionally been used to measure the total delivered dose at a single or multiple points. The steep dose gradient near BT sources has led to large uncertainties in the dose measurements with deviations of more than 30% between planned and measured doses [1–7]. A misplacement of the dosimeter or a nearby source position of only a couple of millimetres can cause high deviations in the measured dose, e.g. 1 mm positional offset at 1 cm leads to a 20% offset in dose. IVD is normally used as an independent assessment of the quality of the treatment. However, the large deviations seen in treatments progressing as planned make the total dose measurements very challenging for quality assurance of the treatment. Consequently, the use of IVD in BT has been limited.

The emergence of new detectors has enabled dose rate measurements with read-out rates shorter than the dwell times [8–11]. This allows for determining the dose rate for each dwell position rather than only the total dose. The ability of determining the dose rate for each dwell position has led to a conceptual change of the role of IVD. Rather than comparing the dose rates directly, the dose rate information can be used to track the source by reconstructing the dwell positions [12–16], determine the most likely detector position [17] and in some cases the dwell time [16,18–21]. The dwell positions and the dwell times together with the source activity are the most important parameters for the dose distribution in BT. Any offset in these parameters will alter the dose distribution, and an accurate determination is therefore a clear way of assuring that the treatment is carried out as planned. Most dose delivery errors in BT are expected to lead to positional offsets; however timing incidences could occur as well. Examples of the latter could be afterloader malfunction or treating with an erroneous source activity. A complete treatment verification system should therefore be able to identify errors both in position and time. Sub-millimetre precision in

Abbreviations: BT, Brachytherapy; DAQ, Data acquisition; EBRT, External beam radiotherapy; HDR, High dose rate; IVD, *in vivo* dosimetry; MR, Magnetic resonance; MRI, Magnetic resonance imaging; OAR, Organs at risk; PMT, Photomultiplier tube; RL, Radioluminescence; SD, Standard deviation

* Corresponding author.
E-mail address: jacjoa@rm.dk (J.G. Johansen).

https://doi.org/10.1016/j.ejmp.2019.03.031
Received 6 December 2018; Received in revised form 22 February 2019; Accepted 29 March 2019
Available online 06 April 2019
1120-1797/ © 2019 Associazione Italiana di Fisica Medica. Published by Elsevier Ltd. All rights reserved.

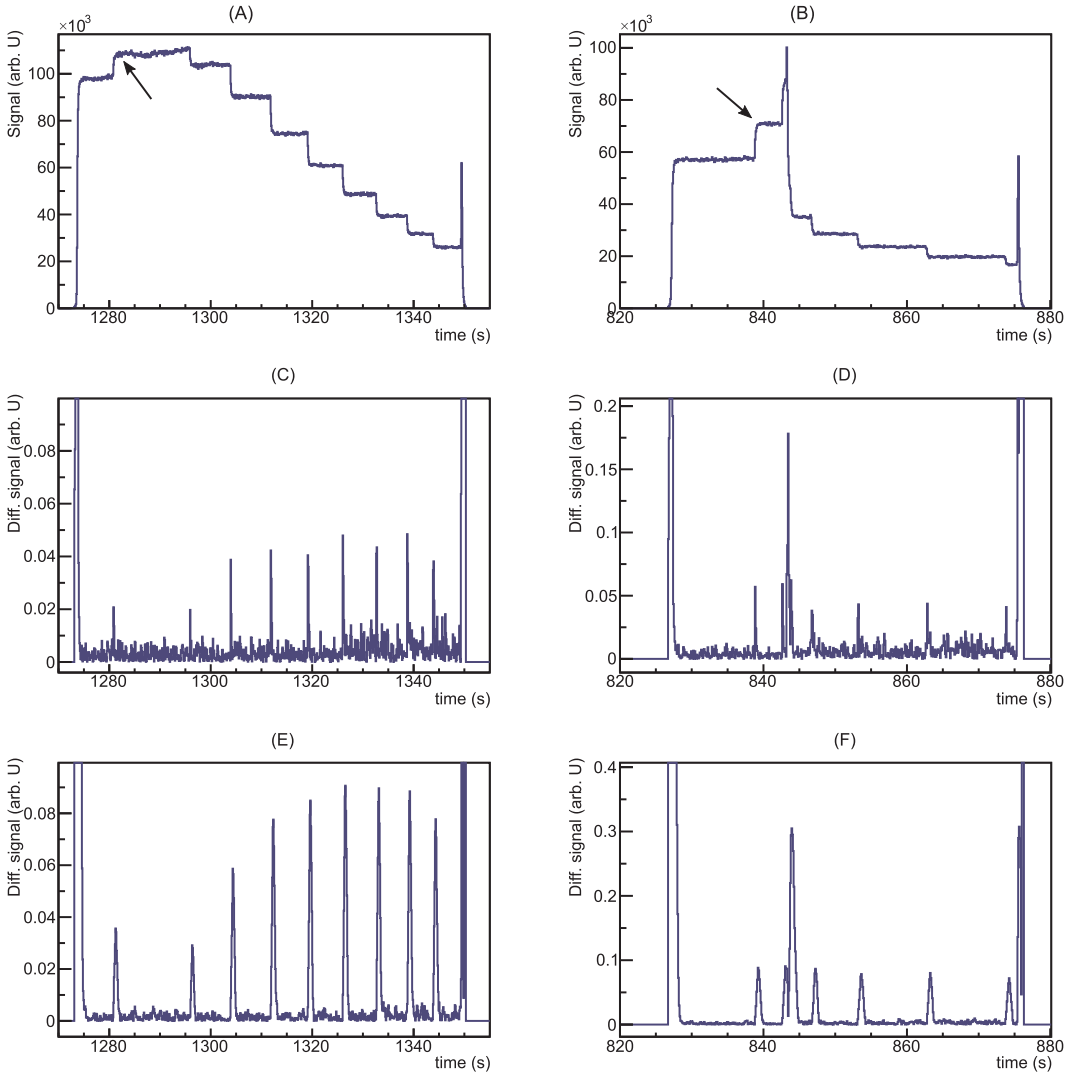

Fig. 1. The measured count rate and the relative difference between two adjacent measurements from two different needles in a single patient treatment. A, C and E corresponds to data from needle 1 and B, D and F needle 2. A and B: Un-calibrated count rate. The arrows indicate shoulders from relaxation of the crystal. C and D: The difference of two adjacent count rate measurements divided by the sum of the two measurements. E and F: The same as C and D but using a running averaging across 5 measurements.

dwell positions and down to 0.001 s in dwell times [18] have been reported in the source tracking studies. However, the majority of the studies have been performed in phantoms in order to demonstrate the precision in a controlled environment. Only few patient studies have been performed [12,15,17,21,22] including a study with 20 high dose rate (HDR) prostate treatments [15] and a study with 2 pulsed dose rate cervix treatments [17], which reported on the use of real-time IVD to perform positional tracking of the BT source and to determine the most likely detector position, respectively. This paper is a continuation of the study with 20 HDR prostate patients [15] focussing on measuring dwell times using data from the treatments for a more complete evaluation of the system. The purpose of this paper is to: 1) characterise the ability of time resolved *in vivo* dosimetry to verify source dwell times and 2) to evaluate the dwell time accuracy of the afterloader during patient treatments.

2. Materials and methods

IVD was performed as part of the clinical workflow in 20 HDR prostate treatments. The measured data was analysed post treatment. A detailed description of the IVD system and the clinical workflow can be found in [15] and will only be described briefly here.

2.1. Detector system

The detector system was based on a small ($0.5 \times 0.5 \times 2\,mm^3$) radio-luminescence (RL) crystal made of Al_2O_3:C. The detector probe consisted of a crystal coupled to a 15 m long fiber-optic cable transmitting the RL-signal to the data acquisition (DAQ) system. The crystal and fiber-optic cable were protected by plastic tubing to provide mechanical robustness and prevent visible light from contaminating the RL-signal. The outer diameter of the detector probe was 1 mm [10] and was therefore sufficiently small to be placed inside a BT plastic needle (6F) during BT. The DAQ-system consisted of a photo multiplier tube (PMT) photon counting device (h7360-01 Hamamatsu, Japan) and a digital interface (NI9402, National Instruments, USA) which converted the RL-signal to a computer-readable count rate signal. A band pass filter (395–440 nm) was used to detect the light about the centre of the Al_2O_3:C RL emission peak. The acquisition rate was 10 Hz for the first ten treatments and was then increased to 20 Hz for the last ten treatments.

2.2. Clinical procedure

The IVD was performed during HDR BT of prostate cancer. Patients

with high- and intermediate risk prostate cancer received a BT boost (17 Gy in two fractions) after external beam radiotherapy (EBRT) (46 Gy in 23 fractions). The needles were inserted using trans-rectal ultrasound guidance. An additional needle intended for the detector was inserted last. The aim was to place the detector needle as close to the centre of the gland as possible while avoiding positions directly adjacent to needles intended for treatment. The needle reconstruction, organ delineation and treatment planning was performed on an MR-image obtained approximately one hour after the needle implantation. The MRI was an axial T2 weighted turbo spin-echo with a 2 mm slice thickness and 1.4 mm × 1.76 mm in-plane resolution [23]. The treatment was planned using a minimum dwell time of 0.1 s and a minimum of 3 mm between successive dwell positions as requirements. A second MR-scan was performed just prior to BT delivery. This MR was used to investigate possible needle migrations. A needle shift > 3 mm led to a re-optimisation of the plan. The dose was delivered using a remote afterloader (Flexitron®, Elekta).

2.3. Data analysis

The dwell times were identified through post-treatment data analysis. The raw count rate was used because the change in signal rather than the dose rate was of interest. The data from the ten treatments with a 20 Hz acquisition rate was analysed twice, once using all data points and once where the average of two adjacent data points was used to resemble a 10 Hz sampling rate. The latter enabled a clearer comparison of all the data points.

When an afterloader source moves from one dwell position to another, the measured count rate will change, as seen in Fig. 1A and B. The movement speed of the source has been determined to be on the order of 30 cm/s [24–26]. This results in a fraction of the sampling rate and is therefore considered as an undetectable change in the measured count rate in this study. The individual dwell times were determined by subtracting two subsequent time instances where large changes in the dose rate occur (transit of the source). These time instances were identified by calculating the difference of two adjacent count rate measurements. The differences were normalised by dividing by the sum of two measurements, resulting in Eq. (1). The normalisation was performed to accommodate for the large difference in signal strength between dwell positions close by and far away.

$$S_i = \left| \frac{C_i - C_{i+1}}{C_i + C_{i+1}} \right| \quad (1)$$

S is the normalised absolute change in count rate between two adjacent measurements, C the count rate, and i the index number of the measurement, corresponding to the measurement time multiplied by the acquisition rate. Fig. 1C and D shows that S_i is close to zero with peaks occurring when the source moved from one dwell position to another. The fluctuation in the signal between the peaks is caused by the noise. This fluctuation increases, when the source is located outside the patient during transfers between two needles. Eq. (1) is therefore employed only while the source is inside a needle and all other measurements were set to 0. The fluctuations induced by noise were reduced by using a running average as shown in eq. (2):

$$S_i = \left| \frac{\sum_{n=i-M}^{i} C_n - \sum_{n=i+1}^{M+i+1} C_n}{\sum_{n=i-M}^{i} C_n + \sum_{n=i+1}^{M+i+1} C_n} \right| \quad (2)$$

M is the number of time points averaged across. A large M will lead to a reduced noise but also broader peaks. The choice of M is therefore a trade-off between signal-to-noise ratio in the detector system and time resolution, which can affect the ability to distinguish shorter dwell times. In this study $M = 5$ and 10 was used for 10 and 20 Hz acquisition rates respectively, corresponding to an averaging over 0.5 s. The choice of M was made based on a short investigation of M-values between 1 and 10 using a single treatment. Since it was a running average, count rate changes were still determined every 0.1 or 0.05 s.

The peaks in the S_i signal, corresponding to the timing of a dwell position change, were identified with the ROOT software (v5.34 CERN) using the built in peak-finder algorithm. The timing was returned in multiples of the acquisition rate (0.1 s and 0.05 s).

For the first and last dwell position in a needle, the transfer time is longer than the transfer times between neighbouring dwell positions. This leads to an extended duration of dose rate changes and therefore a broader peak on the dose rate difference (S_i) plot (Fig. 1C–F). This broadening leads to an increased uncertainty in the determination of the top point and thereby an increased uncertainty in the determination of the dwell time of these dwell positions. This effect is particularly strong for the last position where the source moves from the far end of the needle and out, passing the detector on its way. The timing of the source exit from a needle was therefore determined in an alternative way in order to improve the determination of the dwell time for the last position in a needle. The raw signal was used rather than the difference in dose rates. A sharp peak is seen in the raw signal at the end of each needle, Fig. 1A and B. The peak stems from the fast extraction of the source from the needle where the source passes by the nearest point to the detector. Using this peak as the exit time of the source, increased the precision of the dwell time determination for the last dwell positions in the needles.

All peaks and dwell times were found without prior knowledge of the dose plan. The measured dwell times were matched to the expected ones. The dwell times were separated into two sets: One where a single dwell time was identified and one where the measured dwell time corresponded to the accumulated dwell times of two or more subsequent dwell positions. The prior will be referred to as the identified dwells and the latter referred to as the unidentified ones. The detection efficiency of the system was determined by comparing the number of identified dwell times with the total number. This identification and comparison were done for three data subsets: 1) all dwell positions, 2) for dwell positions with dwell times longer than 1 s and 3) for dwell positions with dwell time shorter than 1 s. The reason for the separation between long and short dwell times is that the time the source is in transit is part of the dwell time. This makes the shorter dwell times harder to identify as the stable period seen in most dwell positions is very short or undetectable. Examples of stable periods are seen in Fig. 1A and B.

The precision of the measurements was determined for all identified dwell positions by subtracting the measured dwell time from the planned ones (dt). The deviations seen were a combination of uncertainties in the determination of the dwell times and the accuracy of the afterloader.

3. Results

Data from a total of 20 treatments in 12 patients were analysed. This involved a total of 3518 dwell positions, 3111 (88%) of which the dwell times were 1 s or longer. In 6 out of the 20 treatments the detector was placed outside the prostate close to the apex. The detector was still close enough to the source positions to provide a useful signal in this study.

3.1. Detection efficiency

Fig. 1 shows both the raw measured count rate and the difference between two adjacent measurements (S_i), for two needles in a single treatment. The difference was calculated both from the raw difference using Eq. (1) (Fig. 1C and D) and from the running average using Eq. (2) (Fig. 1E and F). Application of a running average reduced the noise and broadened the peaks in the plots showing the difference in count rate (panel E compared to C and panel F compared to D). The widths of the peaks were ~0.24 s (1 sigma) when using a running average across 0.5 s.

Table 1
The detection efficiency of dwell times both for each treatment and across all treatments. The efficiency is given both in absolute numbers and percentage. The detection efficiency was determined under three conditions: All dwell times, long dwell times (> =1 s) and short dwell times (< 1 s).

Treatment	All		Dwell times > =1 s		Dwell times < 1 s	
	Identified/total	[%]	Identified/ total	[%]	Identified/total	[%]
1	143/172	83	131/136	96	12/36	33
2	152/166	92	149/155	96	3/11	27
3	169/186	91	164/169	97	5/17	29
4	142/154	92	139/146	95	3/8	38
5	127/186	68	126/153	82	1/33	3.0
6	124/158	78	124/153	81	0/5	0.0
7	145/183	79	145/170	99	0/13	0.0
8	172/223	77	159/169	94	13/54	24
9	156/199	78	151/171	88	5/28	18
10	120/149	81	118/140	84	2/9	22
11	141/143	99	139/139	100	2/4	50
12	123/147	84	118/135	87	5/12	42
13	120/144	83	116/137	85	4/7	57
14	170/217	78	161/190	85	9/27	33
15	164/194	85	164/179	92	0/15	0.0
16	99/139	71	96/124	77	3/15	20
17	133/139	96	132/136	97	1/3	33
18	173/234	74	166/214	78	7/20	35
19	156/226	69	132/154	86	24/72	33
20	141/159	89	137/141	97	4/18	22
All	**2870/3518**	**82**	**2767/3111**	**89**	**103/407**	**25**

Table 1 shows the percentage of dwell positions which could be correctly assigned for each patient treatment. The average detection efficiency was 89% and 25% when considering dwell positions with dwell times longer and shorter than 1 s, respectively. There was no significant change in the detection efficiency when the acquisition rate was increased: 81.4% at 10 Hz and 81.6% at 20 Hz. An investigation of the source positions furthest away from the detector (between 5 cm and 6 cm) showed that 50 out of 51 were identified. The unidentified dwell position corresponded to two adjacent dwell positions with dwell times of 0.5 s and 0.1 s

3.2. Precision

The deviations between measured and expected dwell times (dt) were a multiple of the time resolution (0.1(0.05) s for 10(20) Hz). A histogram of the deviations is shown in Fig. 2. The mean (standard deviation) value of the dt-values were −0.02(0.06) s. A more detailed overview of this is given in Table 2, which shows the percentage of dwell positions where the absolute value of the deviation in dwell times were less than a range of dt-thresholds. The thresholds chosen were based on the time resolution and assuming that the uncertainty of a measured time was ½ the sample rate, e.g. 0.025 s for 20 Hz. The maximum deviation was −0.3 s and −0.4 s for dwell times above and below 1 s, respectively. Measured dwell times were within 0.15 s of the planned dwell time for 97% of the identified dwell times. Further investigation of the 165 dwell positions, where the deviation between measured and planned dwell time were above 0.15 s, showed that 64% (105/165) of these was a first dwell position in a needle. The remaining ones were nearly equally divided between last dwell positions in a needle (16), related to short (< 1 s) dwell times (24) and other positions (17).

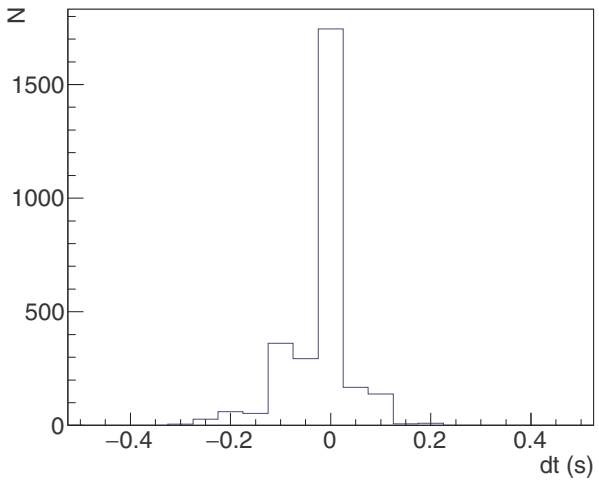

Fig. 2. A histogram of all the deviations between measured and planned dwell times (dt) for all 2870 identified dwell positions. The binning is 0.05 s based on the time resolution of the system.

4. Discussion

4.1. Precision

The precision of the time measurements for the identified dwell positions is very good with 97% of dwell times being within one sampling point (0.15 s). In a similar study, Smith et al. reported on two patient treatment measurements using a flat panel detector [21]. They observed an agreement better than 0.13 s in 78% of the dwell positions. The precision in this study is also comparable to the precision obtained in two other studies. Guiral et al. used four inorganic scintillation detectors in two different configurations (a plastic phantom and an applicator with the detectors implemented in) to track the source and determine the dwell times [16], and Fonseca et al. used an imaging panel to perform similar studies [19]. The first group obtains standard deviations of 0.09 s and 0.08 s for the two configurations and the second group 0.1 s, both slightly higher than the 0.06 s from this study. The maximum absolute deviation was 0.2 s in both studies. Larger deviations were seen in this study, but they were mainly measured in the first dwell positions in a needle. The study by Smith et al. were performed on patient treatments and had sub-second dwell times, but the studies by Guiral et al. and Fonseca et al. had no dwell times below 1 s (shortest dwell time was 6 s), hence it is not known how their methods perform when short dwell times are present. Another study using a pinhole camera showed a mean (1SD) of deviations in time of 0.8 (0.4) s for dwell times of 10 s [20].

4.2. Detection efficiency

The detection efficiency of the system was close to 80%, which means that nearly every fifth dwell time would be unidentified (18% see Table 1). The unidentified dwell positions can be separated into two categories. The first is the short dwell times. Even though dwell times below 0.5 s were identified in a few cases, these events are generally harder to identify. One reason is the fact that the transit time of the source between two dwell positions also counts as part of the dwell time, and for the dwells with a short dwell time, the transit time constitutes a significant part of the total dwell time. This is also the reason, why some clinics set a lower dwell time limit of 1 s. Another reason is the need for a running average. The broadening of the peaks due to the averaging makes the close lying peaks in the plot of the differences around a short dwell time to merge into one, as was seen in Fig. 1F at time ~845 s. Finally, the type of crystal used (Al_2O_3:C) possess a characteristic relaxation time [27,28], which is seen as shoulders in Fig. 1A and B. This delays the stability of the count rate signal and, as a result, less defined S_i-value changes. There are other types of scintillation material, with relaxation times that are insignificant for the purpose of dwell time identification

It is evident from Table 1 that short dwell times cannot explain all unidentified dwell times. The other group of unidentified dwells is due

Table 2
The percentage of determined dwell times for which the absolute deviation between the expected dwell times is within the dt-threshold given in the top row. The percentage is given for all treatments together and for the treatments with a given acquisition rate (ten treatments each). The two rows indicated with 10 Hz in parentheses are the results, when an average of two data point was used for the 20 Hz measurements to resemble 10 Hz measurements.

	$\|dt\| < 0.025$ s	$\|dt\| < 0.05$ s	$\|dt\| < 0.75$ s	$\|dt\| < 0.125$ s	$\|dt\| < 0.15$ s	$\|dt\| < 0.225$ s	$\|dt\| < 0.25$ s
10 Hz		75.4%			98.0%		99.9%
20 Hz	48.6%		78.1%	91.1%		97.9%	
20 Hz (as 10 Hz)		66.3%			96.3%		99.3%
All (as 10 Hz)		70.4%			97.1%		99.6%

to too small changes in dose rate between two successive dwell positions. In this case the dose rate change does not exceed the noise of the system. This can either happen if the distance between the source and the detector is large or when the source passes the point in the given needle with the shortest distance to the detector.

The analysis of the dwell positions furthest away from the detector (> 5 cm) indicates no problem with the dwell positions being too far away from the detector as 98% of dwell times were identified. The latter leads to a top in the count rate pattern as seen in Fig. 1A (at t ~ 1290 s). It is clear that the peaks in Fig. 1C and E are smaller close to the top of the signal in Fig. 1A.

Finally the dose rates may fluctuate if the dosimeter or source moves during a dwell, e.g. due to patient movement. If the movement is large enough, it can either hide a source movement or resemble a movement leading to a wrong identification of shift in dwell position. However, in our study such fluctuations were generally very small, because the dosimeter was placed inside a needle that was attached to the implant of the source needles. The dosimeter moved therefore together with the other needles in relation to patient motion. This is why we did not observe variations attributable to patient movement.

4.3. Limitations

The major limitation of the system is the detection efficiency, which was mainly related to: 1) dwell times of < 1 s and 2) neighbouring source positions with similar dose rate. In general the most important factor for improving the detection efficiency is the signal to noise ratio. An improved signal to noise ratio will allow for a reduced number of elements (*M*) in the running average and would at the same time enable a clearer identification of dwells with dose rate close to each other. However, to fully improve on resolving dwell times for neighbouring source positions with similar dose rates at least two detectors are required as done by Guiral et al. [16]. Furthermore, the measurement of the first dwell positions in the needles generally had larger uncertainties than the other dwell positions A more elaborate determination of the dwell time than performed in this study could improve the precision further.

4.4. Brachytherapy incidences related to dwell timing

A report from IAEA published in 2000 contained 38 BT errors [29]. Twelve of them were due to either wrong activity or isotope, which would lead to a wrong dwell time. However, the incidences could also be identified by means of a direct comparison between the measured and delivered doses as long as the detector calibration was independent from the wrong activity or isotope. Similar experiences were reported in incidence reports by the UK government [30]. The reports list 40 BT incidences from 2017. Two of these were related to wrong source activity, and the remaining incidences were related to wrong planning or source positions. Eight incidences were reported as “others” and could potentially be dwell time related. This indicates that incidences involving wrong dwell times rarely occur in BT and the focus on treatment verification should be on identifying positional offsets. Nonetheless, studies, including this one, show that dwell time errors can be identified.

4.5. Clinical impact

This study has shown that dwell times can be determined with sufficiently high precision to be used for error detection in BT, although the detection efficiency should be improved before using the technique clinically for online monitoring of dwell times. Dwell time accuracy of 0.2 s, which is the current limit of the system in this study, is sufficient to avoid dosimetric variations related to timing which could have clinical impact. The study also showed that the dwell times were very stable. The attention of BT treatment verification should therefore be focussed on verification of the source positions.

5. Conclusion

Dwell times can be assessed with high accuracy with the use of time resolved *in vivo* dosimetry. The accuracy and precision obtained in this study enable a detection of dwell time offsets with clinical impact. However the detection efficiency should ideally be improved to avoid false errors. The analysis furthermore demonstrates stability of dwell timing over more than 3000 dwell times, over 20 patients, and during a period of one year, which indicates that dwell time offsets is a minor source of uncertainty in BT.

Acknowledgements

We wish to thank Dr. M.S. Akselrod, Stillwater Crystal Growth Division, Landauer Inc, USA for the Al2O3:C crystals. This study was supported by unrestricted research grants from Elekta, Novo Nordisk Foundation and by the Danish Cancer Society.

Appendix A. Supplementary data

Supplementary data to this article can be found online at https://doi.org/10.1016/j.ejmp.2019.03.031.

References

[1] Jaselske E, Adliene D, Rudzianskas V, Urbonavicius BG, Inciura A. In vivo dose verification method in catheter based high dose rate brachytherapy. Phys Med 2017;44:1–10.
[2] Carrara M, Romanyukha A, Tenconi C, et al. Clinical application of MOSkin dosimeters to rectal wall in vivo dosimetry in gynecological HDR brachytherapy. Phys Med 2017;41:5–12.
[3] Waldhausl C, Wambersie A, Potter R, Georg D. In-vivo dosimetry for gynaecological brachytherapy: physical and clinical considerations. Radiother Oncol 2005;77(3):310–7.
[4] Brezovich IA, Duan J, Pareek PN, Fiveash J, Ezekiel M. In vivo urethral dose measurements: a method to verify high dose rate prostate treatments. Med Phys 2000;27(10):2297–301.
[5] Anagnostopoulos G, Baltas D, Geretschlaeger A, et al. In vivo thermoluminescence dosimetry dose verification of transperineal 192Ir high-dose-rate brachytherapy using CT-based planning for the treatment of prostate cancer. Int J Radiat Oncol Biol Phys 2003;57(4):1183–91.
[6] Das R, Toye W, Kron T, Williams S, Duchesne G. Thermoluminescence dosimetry for

in-vivo verification of high dose rate brachytherapy for prostate cancer. Aust Phys Eng Sci Med 2007;30(3):178–84.
[7] Suchowerska N, Jackson M, Lambert J, Yin YB, Hruby G, McKenzie DR. Clinical trials of a urethral dose measurement system in brachytherapy using scintillation detectors. Int J Radiat Oncol Biol Phys 2011;79(2):609–15.
[8] Therriault-Proulx F, Beddar S, Beaulieu L. On the use of a single-fiber multipoint plastic scintillation detector for 192Ir high-dose-rate brachytherapy. Med Phys 2013;40:062101.
[9] Wang R, et al. Implementation of GaN based real-time source position monitoring in HDR brachytherapy. Rad Med 2014;71:293–6.
[10] Andersen CE, et al. Characterization of a fiber-coupled Al_2O_3: C luminescence dosimetry system for online *in vivo* dose verification during $^{19}2$Ir brachytherapy. Med Phys 2009;36:708–18.
[11] Kertzscher G, Beddar S. Inorganic scintillator detectors for real-time verification during brachytherapy. J Phys: Conf Ser 2017;847:012036.
[12] Tanderup K, et al. Geometric stability of intracavitary pulsed dose rate brachytherapy monitored by in vivo rectal dosimetry. Rad Oncol 2006;79:87–93.
[13] Smith RL, et al. Source position verification and dosimetry in HDR brachytherapy using an EPID. Med Phys 2013;40(11):111706.
[14] Therriault-Prouix F, et al. On the use of a single-fiber multipoint plastic scintillation detector for 192 Ir high-dose-rate brachytherapy. Med Phys 2013;40(6):062101.
[15] Johansen JG, et al. Time-resolved in vivo dosimetry for source tracking in brachytherapy. Brachytherapy 2018;17:122–32.
[16] Guiral P, et al. Design and testing of a phantom and instrumented gynecological applicator based on GaN dosimeter for use in high dose rate brachytherapy quality assurance. Med Phys 2016;43(9):5240–51.
[17] Kertzscher G, et al. Adaptive error detection for HDR/PDR brachytherapy: guidance for decision making during real-time in vivo point dosimetry. Med Phys 2014;41(5):052102.
[18] Espinoza A, et al. The feasibility study and characterization of a two-dimensional diode array in “magic phantom” for high dose rate brachytherapy quality assurance. Med Phys 2013;40(11):111702.
[19] Fonseca GP, et al. Online pretreatment verification of high-dose rate brachytherapy using an imaging panel. Phys Med Biol 2017;62:5440.
[20] Watanabe Y, et al. Automated source tracking with a pinhole imaging system during high-dose-rate brachytherapy treatment. Phys Med Biol 2018;63:145002.
[21] Smith RL, et al. An integrated system for clinical treatment verification of HDR prostate brachytherapy combining source tracking with pretreatment imaging. Brachytherapy 2018;17:111–21.
[22] Andersen CE, Nielsen SK, Lindegaard JC, Tanderup K. Time-resolved *in vivo* luminescence dosimetry for online error detection in pulsed dose-rate brachytherapy. Med Phys 2009;36:5033–43.
[23] Buus S, et al. Learning curve of MRI-based planning for high-dose-rate brachytherapy for prostate cancer. Brachytherapy 2016;15:426–34.
[24] Bastin KT, Podgorsak MB, Thomadsen BR. The transit dose component of high dose rate brachytherapy: direct measurements and clinical implications. Int J Radiat Oncol Biol Phys 1993;26:695–702.
[25] Houdek PV, et al. Dose determination in high dose-rate brachytherapy. Int J Radiat Oncol Biol Phys 1992;24:795–801.
[26] Fonseca G, et al. HDR 192Ir source speed measurements using a high speed video camera. Med Phys 2015;42:412–5.
[27] Peto A, Kelemen. A Radioluminescence properties of alpha-Al2O3 TL dosimeters. Radiat Prot Dosim 1996;65(1–4):139–42.
[28] Andersen CE, et al. An algorithm for real-time dosimetry in intensity-modulated radiation therapy using the radioluminescence signal from Al_2O_3:C. Radiat Prot Dosim 2006;120(1–4):7–13.
[29] IAEA, “Lessons learned from accidental exposures in radiotherapy,” IAEA Safety Report Series 17 (IAEA, Vienna, 2000).
[30] UK GOV, Radiotherapy Errors and Near Misses Data Report, URL: https://www.gov.uk/government/publications/safer-radiotherapy-error-data-analysis-report.